Supplementary Information (SI) for ChemComm.
This journal is © The Royal Society of Chemistry 2024

Supporting Information

Topochemically synthesized Nb_3VS_6 as a stable anode for sodium-ion batteries

Harshit Pandey,[a] Pallellappa Chithaiah,[b] Savithri Vishwanathan,[a] H. S. S. Ramakrishna Matte*[a] and C. N. R. Rao*[b]

a. Energy Materials Laboratory, Centre for Nano and Soft Matter Sciences, Bangalore 562162, India.

b. New Chemistry Unit, International Centre for Materials Science and School of Advanced Materials, Jawaharlal Nehru Centre for Advanced Scientific Research, Jakkur PO, Bangalore-560064, India.

*Email: matte@cens.res.in and cnrrao@jncasr.ac.in

Experimental

Synthesis of Nb-HDA complex

Niobium (V) ethoxide (99.95%, Sigma Aldrich), vanadium pentoxide, hydrogen peroxide (30% H_2O_2), and 1-hexadecylamine ($C_{16}H_{33}NH_2$, HDA) were utilized to synthesize the Nb-V-HDA complex. 0.5 ml of niobium (V) ethoxide was dispersed in a 25 ml solution of H_2O_2, followed by the addition of 0.27 g of V_2O_5, resulting in a brown solution. This mixture was then heated to 70^0 C after which a solution of 1.9 g of HDA in 5 ml of ethanol was added. This process led to the spontaneous formation of a Nb-V-HDA complex foam, with heat evolution. The resulting ultra-light foam was collected by filtration, washed with acetone, and dried at room temperature.

Synthesis of Nb_3VS_6 nanosheets

Nb_3VS_6 nanosheets were synthesized from the Nb-V-HDA complex using a horizontal tubular furnace at a temperature of 950^0 C. The reaction process involved a mixture of gases- N_2 (a carrier gas) and H_2S (a reactive gas). First, the Nb-V-HDA complex was taken in a quartz boat and placed at the entrance of the quartz tube, away from the hot zone of the furnace. The temperature of the furnace was then slowly increased to 950^0 C under a continuous flow of N_2 gas with a flow rate of 95 $cm^3\ min^{-1}$ to achieve an oxygen-free atmosphere. Once the furnace temperature was stabilized, the quartz boat containing the Nb-V-HDA complex was carefully pushed into the reaction hot zone of the furnace. The flow rates of N_2 and H_2S gases were set to 65 and 35 $cm^3\ min^{-1}$, respectively. The reaction was allowed to proceed for 45 minutes. After 45 minutes, the boat was removed from the hot zone and placed in the cooler part of the quartz tube. The flow rates of N_2 and H_2S gases were then changed to 85 and 10 $cm^3\ min^{-1}$, respectively, for 30 minutes. Finally, to complete the reaction, the furnace was gradually cooled down to room temperature under N_2 flow.

Characterization

The X-ray diffraction pattern (XRD) was acquired using Rigaku SmartLab and PANalytical X-pert PRO X-ray diffractometers (Cu Kα source (λ = 0.154178 nm)). X-ray photoelectron spectra (XPS) measurements were carried out using an Omicron nanotechnology spectrometer with Mg Kα as the X-ray source. Field emission scanning electron microscopy (FESEM) was carried out using Tescan and Bruker MIRA 3. The transmission electron microscope (TEM) images were

obtained using TALOS F200S G2. Brunauer–Emmett–Teller (BET) measurements were carried out using a Belsorp-Max II instrument and N_2 as the adsorptive gas.

Electrochemical measurements

2032-type coin cells were fabricated in an Ar-filled glovebox with Nb_3VS_6 as working electrode, Na metal as counter electrode using glass fibre separator. A slurry was prepared by grinding Nb_3VS_6, conducting carbon and sodium polyacrylate (PAA) binder in 70:15:15 ratio in deionized (DI) water for 30 min. Blade-coating technique is employed to fabricate thin film of 30 µm thickness on a carbon coated Al (Al-C) foil, followed by drying in a vacuum oven at 110 ^oC for 24 h. 1 M $NaClO_4$ in ethylene carbonate (EC) and propylene carbonate (PC) mixed solvent in the ratio (1:1 vol%) was used as the electrolyte. Neware BTS-4000 battery tester was employed to perform the GCD experiments at different current densities in the voltage range 0.01-2.5 V (vs. Na/Na^+). Metrohm Autolab PGSTAT302N electrochemical workstation was used to carry out EIS and CV measurements. The values of specific capacities and current densities have been determined considering the mass of the active material.

Electrokinetic analysis of Na-ion storage

The functional relation defining the capacitive and diffusive components of the observed current with respect to scan rate is given as:

$$i = k_1 v + k_2 v^{½} \qquad (1)$$

Where v is the scan rate ($V\ s^{-1}$), i is the current (A), and k_1 and k_2 are the constants. The capacitive contribution to the total current is evaluated from k_1v, while the diffusion-controlled current is derived from $k_2v^{1/2}$.

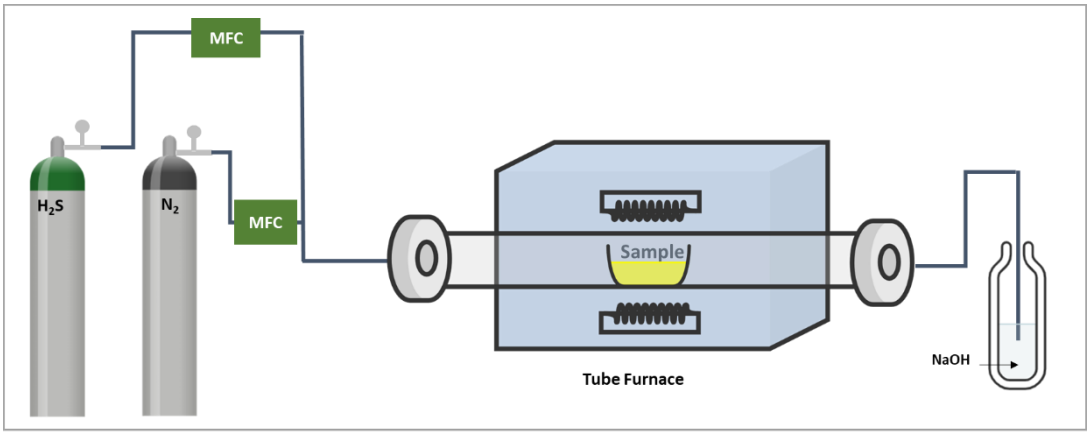

Figure S1 Schematic diagram for synthesis of Nb_3VS_6

Formation mechanism of Nb_3VS_6

In the formation process, the dissolution of niobium ethoxide and vanadium pentoxide in hydrogen peroxide leads to the formation of a brown solution of peroxoniobic and peroxovanadic acids. The addition of HDA solution into the acid solution led to the generation of a yellow-coloured Nb-V-HDA foam. The condensation of peroxoniobic and peroxovanadic acids and the intercalation of HDA occur simultaneously because of the interaction between negatively charged $NbVO_5$ layers and protonated HDA molecules, leading to the formation of 2D $NbVO_5$-HDA (Nb-V-HDA) nanosheets. A similar mechanism was observed for the formation of MoO_3 and Nb_2O_5.[1,2] The structure and the arrangement of the HDA molecules in the Nb-V-HDA complex were determined by X-ray diffraction (Figure S2a). The diffraction peaks at lower angles (5-10^0) Fig S2(a) indicate the inorganic/organic hybrids of Nb-V-HDA lamellar mesostructures of $NbVO_5$. The XRD pattern shows a diffraction peak at 2Θ ~ 21.8˚which corresponds to the (111) planes of the orthorhombic $NbVO_5$ phase (JCPDF No. 00-046-0046).[3,4] It is believed that HDA molecules were intercalated between the $NbVO_5$ crystallites. On subsequent calcination of the Nb-V-HDA complex at high temperature in an inert atmosphere, with H_2S a reactive gas, a sulfurization reaction occurs leading to the formation of pure Nb_3VS_6 nanosheets.

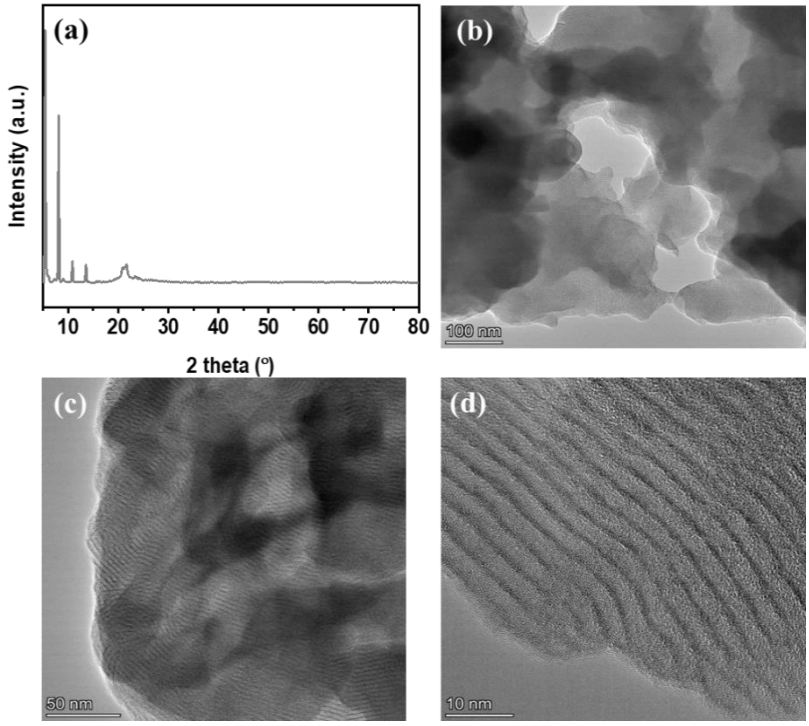

Figure S2 (a) XRD pattern of Nb-V-HDA complex, (b), (c) and (d) TEM images obtained for Nb-V-HDA complex having layered morphology.

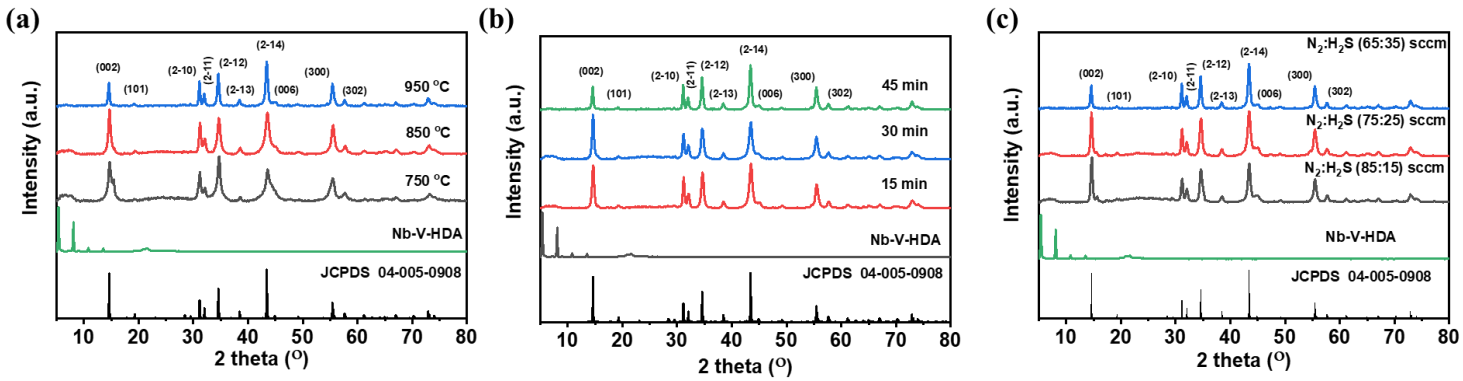

Figure S3 (a) XRD pattern of Nb-V-HDA complex and Nb_3VS_6 under different conditions by varying temperature (750^0, 850^0 and 950^0 C) for 45 minutes at a H_2S flow rate of 35 sccm (b) by varying time (15,30 and 45 min) at 950^0 C at a H_2S flow rate of 35 sccm and (c) by varying H_2S flow rates (15,25 and 35 sccm) at 950^0 C for 45 minutes.

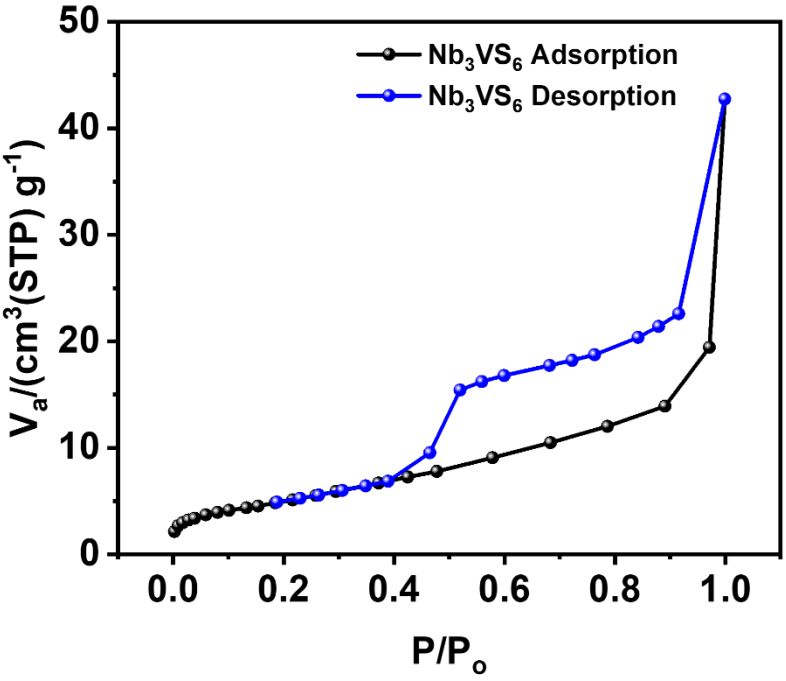

Figure. S4 Adsorption-desorption isotherm of Nb_3VS_6.

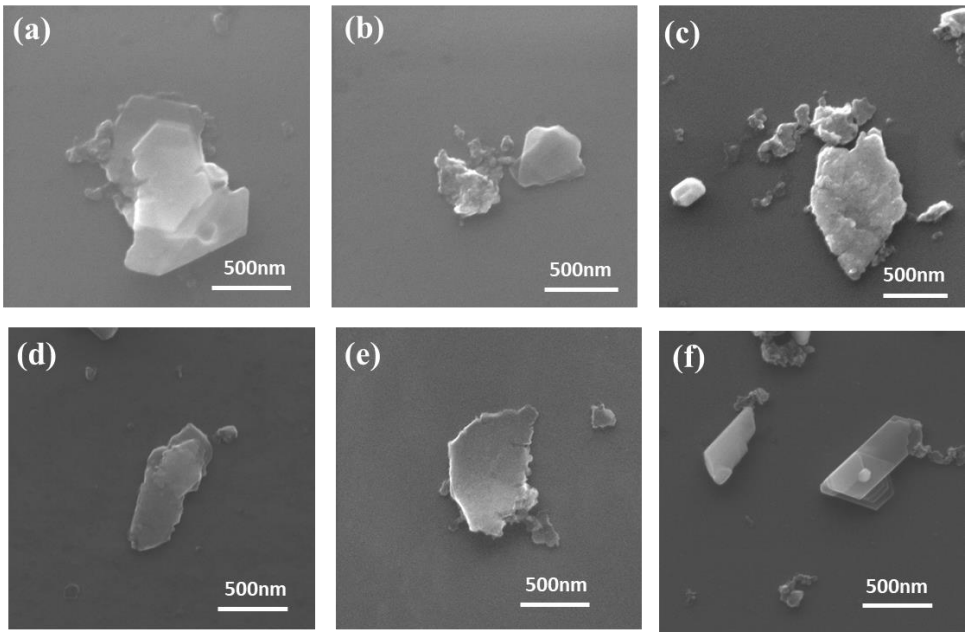

Figure S5. FESEM images of (a,b) Nb_3VS_6 at 750 and 850^0 C respectively, (c,d) Nb_3VS_6 at 15 and 30 min respectively, and (e,f) Nb_3VS_6 at 15 and 25 sccm flow rates respectively.

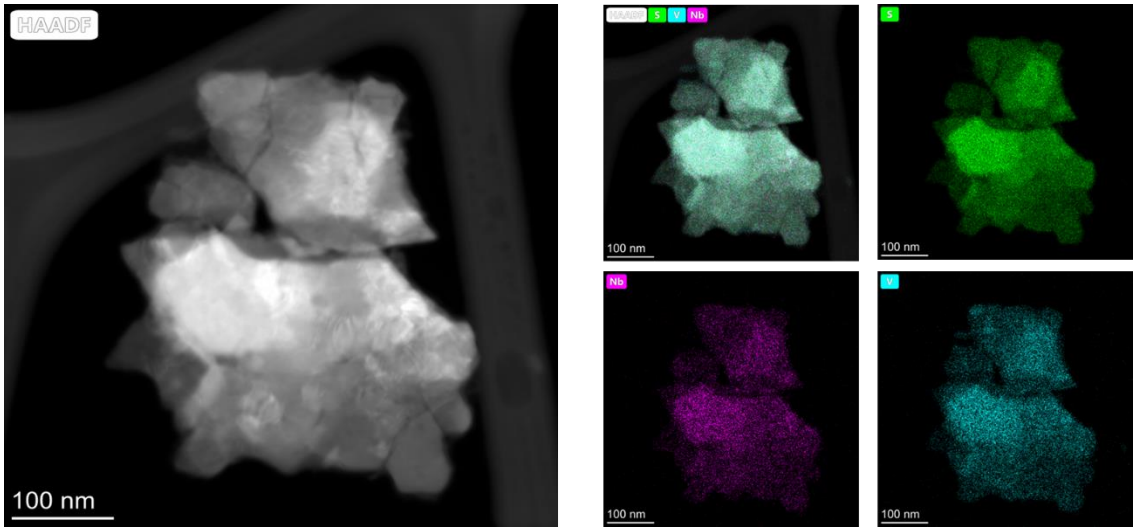

Figure S6 Elemental mapping using HAADF-STEM of Nb_3VS_6.

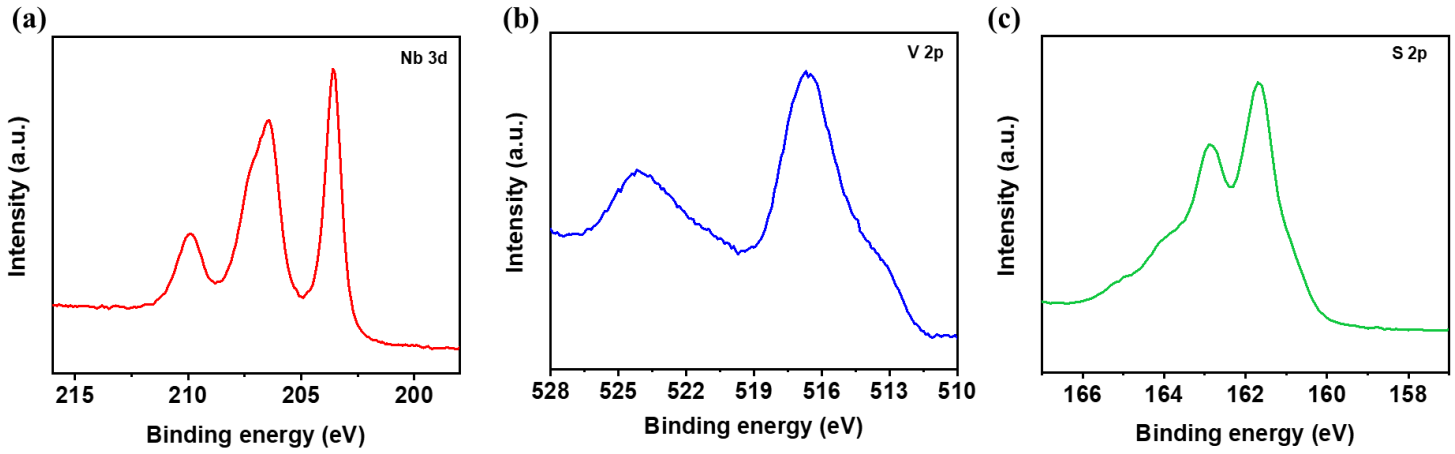

Figure S7 XPS spectra of Nb_3VS_6 (a) Nb 3d, (b) V 3p and (c) S 2p.

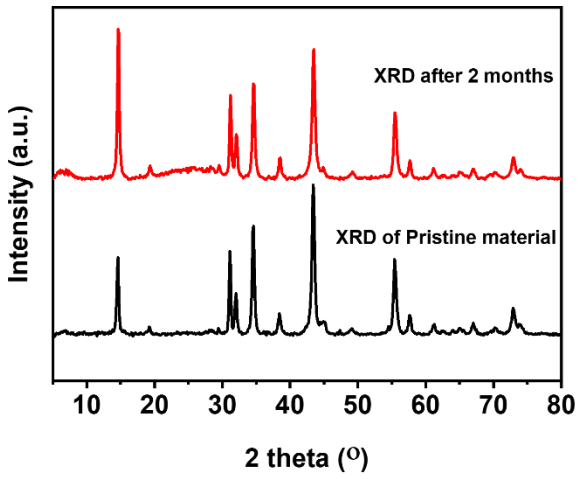

Figure S8 XRD pattern of Nb_3VS_6 kept stored under ambient conditions before and after a span of two months.

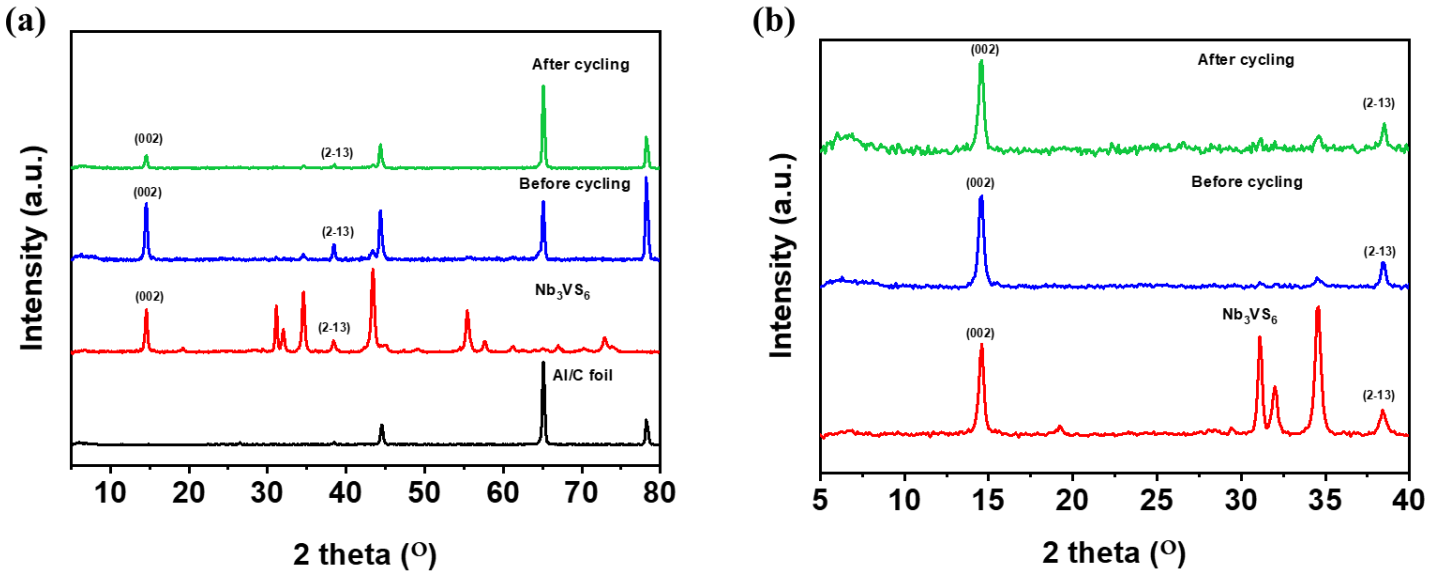

Figure S9 (a) Post-mortem XRD analysis for Nb_3VS_6 before cycling and after 5 cycles, (b) Inset showing comparison between the bulk material with the pre and post cycling XRD pattern showing no considerable changes before and after cycling providing another conclusive proof about the insertion mechanism in Nb_3VS_6.

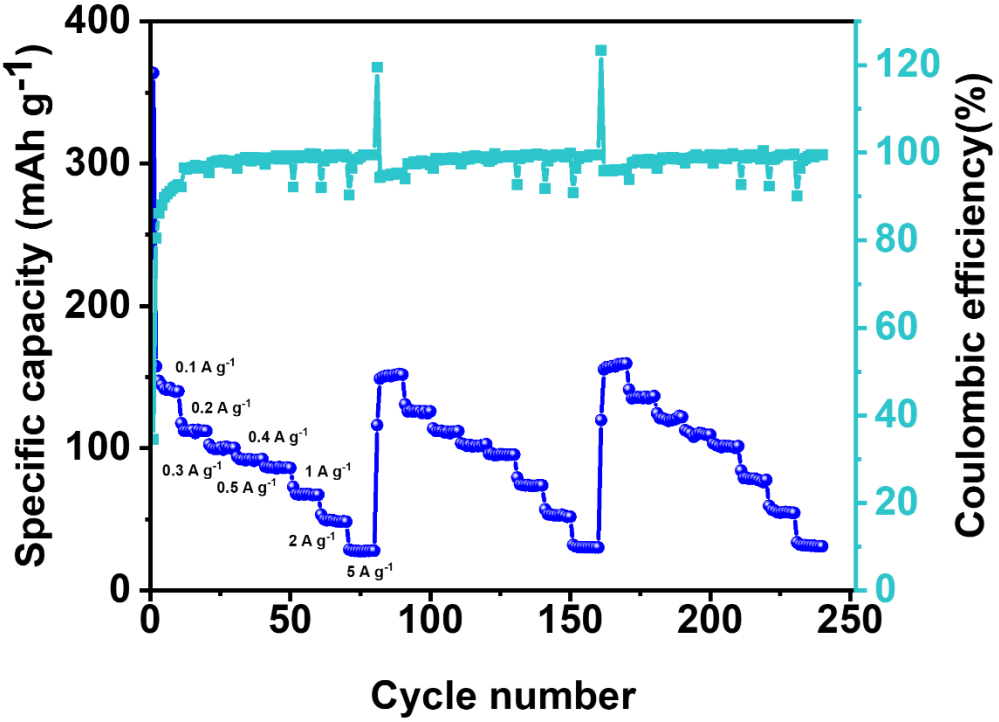

Figure S10 High-rate performance of Nb_3VS_6 SIB anode.

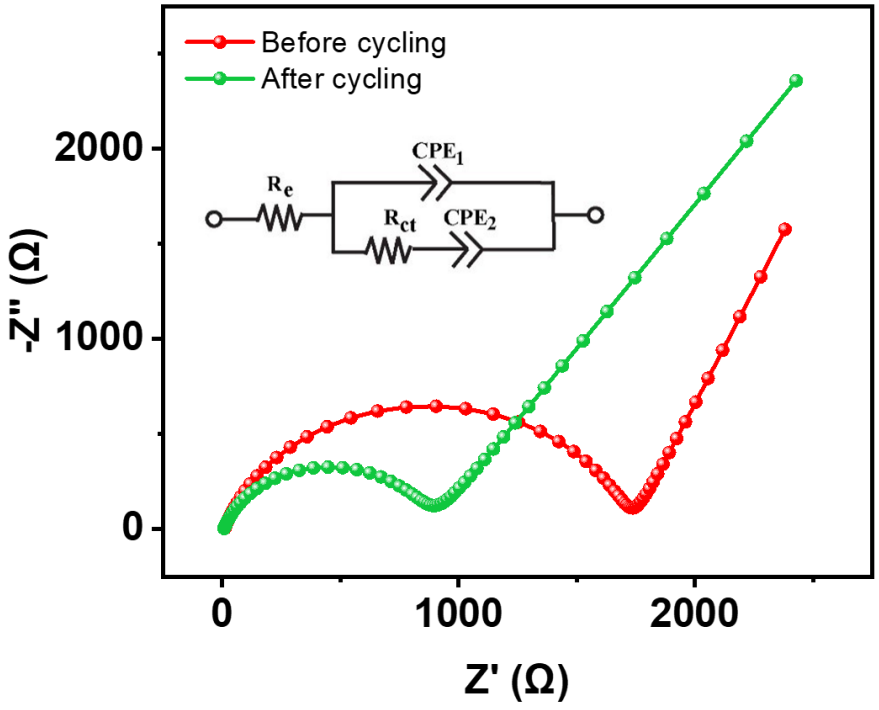

Figure S11 EIS spectra before and after CV cycles at 0.1 mV s^{-1}.

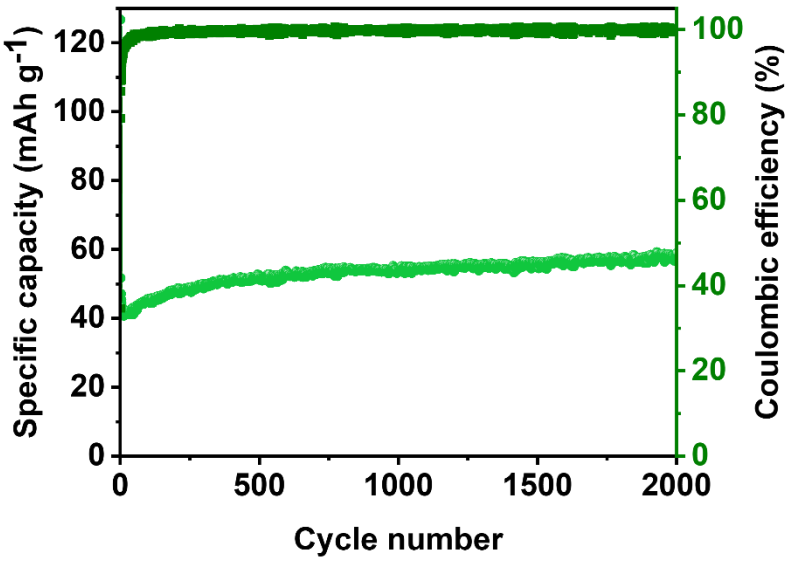

Figure S12 Cycling stability at 2 A g^{-1} for 2000 cycles.

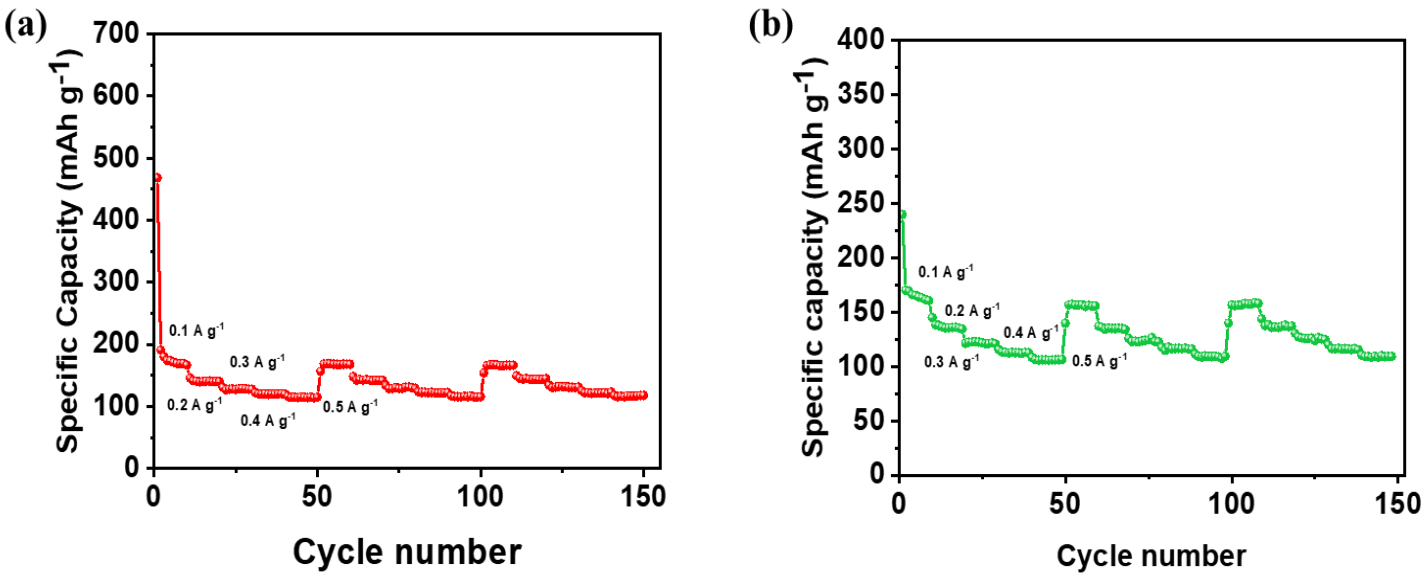

Fig. S13 Rate capabilities of other control samples in SIB (a) with H_2S flow rate of 25 sccm with 950^0 C for 45 minutes, (b) with H_2S flow rate of 35 sccm with 950^0 C for 30 minutes.

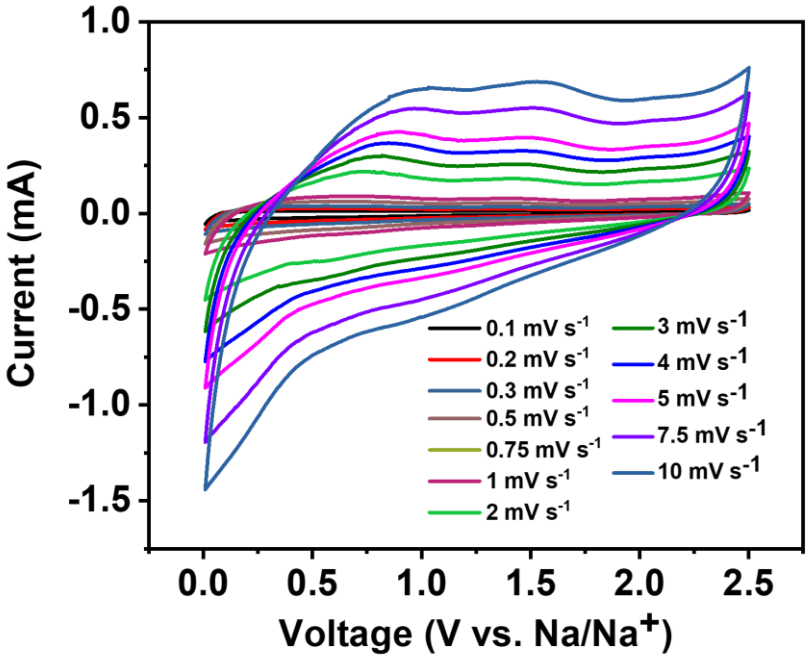

Figure S14 CV of Nb_3VS_6 SIB anode at different scan rates.

Table S1 Comparison of cycling stability performance of Nb_3VS_6 anode with literature

S no	Anode material	Capacity/ Current density	No. of cycles	ref
1	T-Nb_2O_5@NbS_2@C	102 mAhg^{-1} / 2 Ag^{-1}	500 cycles	5
2	SnS/$SnSe_2$	580 mAhg^{-1} / 0.1 A g^{-1}	100 cycles	6
3	N-MoS_2/C@SiOC	486.8 mAhg^{-1} / 0.1 A g^{-1}	200 cycles	7
4	SnS_2/rGO/SnS_2	1133 mAhg^{-1} / 0.1 A g^{-1}	100 cycles	8
5	F-CoSnS	450 mAh g^{-1}/ 0.05 A g^{-1}	200 cycles	9
6	CuV_2S_4	580 mAh g^{-1}/ 0.7 A g^{-1}	300 cycles	10
7	Nb_3VS_6	101.10 mAhg^{-1} / 0.5 A g^{-1}	2500 cycles	This work

References

1 P. Chithaiah, D. C. Binwal and C. N. R. Rao, *Eur. J. Inorg. Chem*, 2022, **2022**, e202101086.

2 R. Singh, P. Chithaiah and C. N. R. Rao, *Nanotechnology*, 2023, **34**, 145705.

3 N. Krins, J. D. Bass, D. Grosso, C. Henrist, R. Delaigle, E. M. Gaigneaux, R. Cloots, B. Vertruyen and C. Sanchez, *Chem Mater*, 2011, **23**, 4124–4131.

4 M. W. Louie and A. T. Bell, *J Am Chem Soc*, 2013, **135**, 12329–12337.

5 C. Pan, J. Kang, Q. Xie, Q. Li, W. Yang, H. Zou and S. Chen, *ACS Appl Energy Mater*, 2021, **4**, 12365–12373.

6 T. Wang, D. Legut, Y. Fan, J. Qin, X. Li and Q. Zhang, *Nano Lett*, 2020, **20**, 6199–6205.

7 H. Lim, S. Yu, W. Choi and S. O. Kim, *ACS Nano*, 2021, **15**, 7409–7420.

8 Y. Jiang, D. Song, J. Wu, Z. Wang, S. Huang, Y. Xu, Z. Chen, B. Zhao and J. Zhang, *ACS Nano*, 2019, **13**, 9100–9111.

9 S. Dou, J. Xu, H. M. K. Sari, H. H. Wu, J. Hu, Y. Zhang, L. Fan, D. Xiong, W. Zhou, Y. Chen and X. Li, *ACS Appl. Mater. Interfaces*, 2020, **12**, 41546–41556.

10 M. Krengel, A. L. Hansen, M. Kaus, S. Indris, N. Wolff, L. Kienle, D. Westfal and W. Bensch, *ACS Appl. Mater. Interfaces*, 2017, **9**, 21282–21291.